A Two-Current Model for the Dynamics of Cardiac Membrane

COLLEEN C. MITCHELL* AND DAVID G. SCHAEFFER
Department of Mathematics,
Duke University and Center for Nonlinear and Complex Systems,
Durham NC 27708,
Box 90320,
U.S.A.

E-mail: dgs@math.duke.edu

In this paper we introduce and study a model for electrical activity of cardiac membrane which incorporates only an inward and an outward current. This model is useful for three reasons: (1) Its simplicity, comparable to the FitzHugh–Nagumo model, makes it useful in numerical simulations, especially in two or three spatial dimensions where numerical efficiency is so important. (2) It can be understood analytically without recourse to numerical simulations. This allows us to determine rather completely how the parameters in the model affect its behavior which in turn provides insight into the effects of the many parameters in more realistic models. (3) It naturally gives rise to a one-dimensional map which specifies the action potential duration as a function of the previous diastolic interval. For certain parameter values, this map exhibits a new phenomenon—subcritical alternans—that does not occur for the commonly used exponential map.

© 2003 *Society for Mathematical Biology. Published by Elsevier Ltd. All rights reserved.*

1. INTRODUCTION

Progress in treating heart disease, especially ventricular fibrillation, requires understanding the electrical behavior of cardiac membrane. Early extensions of the Hodgkin–Huxley equations to cardiac cells were introduced for the Purkinje fiber [see, for example, Noble (1960, 1962)]. Beeler and Reuter (1977) introduced the first model for the dynamics of a ventricular myocyte (myocardial fiber), also based on the ideas of Hodgkin and Huxley. More complicated models [e.g., Luo and Rudy (1991, 1994)], based on sophisticated experiments, including single-cell and single-channel measurements, were developed later. In part of a larger study, Fenton and Karma (1998) attempted to extract a model of minimal complexity that quantitatively reproduced the restitution behavior of more physiological models. Their model contains three currents, loosely corresponding to sodium, calcium, and potassium currents. Carrying their simplifications one step further, in this paper

---

*Author to whom correspondence should be addressed.

we introduce and study a model with just two currents that at least qualitatively reproduces restitution behavior. The equations we derive may be obtained, after various rescalings, as a special case of equations introduced by Karma (1994).

This model is useful for both pedagogical and scientific reasons. On the pedagogical side: (i) The model provides a good introduction to membrane dynamics for a reader more comfortable with mathematics than physiology. (ii) Even for experts in cardiology, our analysis may have interest as an illustration of how asymptotic analysis can simplify complicated models for membrane dynamics. [For example, in Tolkacheva *et al*. (2002), a one-dimensional map to approximate the response of the Fenton–Karma model (Fenton and Karma, 1993) is derived with these techniques.] Because of our desire to foster interdisciplinary communication, we give a more detailed discussion than the sophisticated reader will need.

On the scientific side: (i) An explicit formula for the restitution curve can be derived from the model; thus the response of the model can be described by an iterated map. The restitution curve is qualitatively similar to the commonly used exponential restitution curve. (ii) Because of its simplicity, the model can be understood analytically without recourse to numerical simulations. This allows one to determine rather completely how the various parameters in the model affect its behavior (see Section 5), thereby providing insight into more realistic models. (iii) The simplicity of the model may facilitate computation-intensive simulations of spatially extended tissue. Incidentally, we find (in Section 5) that alternans can occur in this model[†] either supercritically [the usual form that occurs, for example, with the exponential map Nolasco and Dahlen (1968)] or subcritically. We discuss the implications that the latter form of alternans would have for experiments.

The remainder of this paper is organized as follows. The model, a system of two ordinary differential equations, is introduced in Section 2. In Section 3, applying asymptotic analysis, we extract a restitution curve (more accurately, a restitution function) from the ordinary differential equations. In Section 4, following Guevara *et al*. (1984), we formulate the response of the model to periodic stimulation as a bifurcation problem. Finally, in Section 5 we classify the bifurcation diagrams that can occur in this model as a function of its parameters, where by *bifurcation*

[†]In using the standard cardiology term 'alternans' we do not mean to imply that the model is an accurate representation of this phenomenon in membrane dynamics. Rather, we believe that one may learn from a slightly unrealistic model that is simple enough to analyze. For example, the model has pointed to different behavior that may have gone undetected in more realistic models. It should be pointed out that this paper studies *electrical* alternans. Some authors [e.g., Euler (1999)] hold that alternans has a purely mechanical origin, that electrical alternans is a derivative phenomenon. In support of the independence of electrical alternans, let us cite the following:

- In Banville and Gray (2002), two drugs that suppress muscular contraction and thus abolish mechanical alternans are administered, but (electrical) alternans are still observed. The same behavior is reported in Hall *et al*. (1999).
- Purkinje fibers undergo much less contraction than other heart tissue, but alternans is still observed in these fibers [see for example Gilmour *et al*. (1997)].

diagram we mean the graph of action-potential duration as a function of the period of the stimuli. This classification is obtained with purely analytical means.

2. THE MODEL

The model contains two functions of time, the transmembrane potential or voltage $v(t)$ and a gating variable $h(t)$, and these satisfy ordinary differential equations. In the language of physiology, our model may be described as a *uniformly polarized membrane patch*; it may be viewed as describing the dynamics of a spatially clamped ventricular myocyte. The model may be obtained after appropriate rescaling as a special case of Karma (1994).

The voltage, which is dimensionless and scaled so that it ranges between zero and one[‡] is governed by the ODE

$$\frac{dv}{dt} = J_{\text{in}}(v, h) + J_{\text{out}}(v) + J_{\text{stim}}(t), \tag{1}$$

where the three currents J_{in}, J_{out}, and J_{stim} have the following descriptions: (i) The inward current J_{in}, a combination of all currents which raise the voltage across the membrane (primarily sodium and calcium), is given by

$$J_{\text{in}}(v, h) = \frac{hC(v)}{\tau_{\text{in}}}, \tag{2}$$

where the cubic function $C(v) = v^2(1-v)$ describes the voltage dependence of the inward current. This voltage dependence, taken in modified form from the Fenton–Karma model, mimics the behavior of the fast acting gates in more complicated models such as Luo and Rudy (1991). In our scaled variables, the strength of J_{in} is specified by the time constant τ_{in}. The behavior of h as a gate—open when $h = 1$, closed when $h = 0$—may be seen from equation (2). The evolution of h is governed by equation (4) below. (ii) The outward current J_{out}, a combination of the currents which decrease the membrane voltage (primarily potassium), is given by

$$J_{\text{out}} = -\frac{v}{\tau_{\text{out}}}; \tag{3}$$

this current is ungated. (iii) The stimulus current, J_{stim}, is an external current applied in brief pulses by the experimenter as specified below.

The gating variable h, which is dimensionless and varies between 0 and 1, satisfies the ODE

$$\frac{dh}{dt} = \begin{cases} \frac{1-h}{\tau_{\text{open}}} & \text{if } v < v_{\text{gate}} \\ \frac{-h}{\tau_{\text{close}}} & \text{if } v > v_{\text{gate}} \end{cases} \tag{4}$$

[‡]The voltage may be scaled back to the original physiological values using the change of variables $\bar{v} = v_{\text{min}} + v(v_{\text{max}} - v_{\text{min}})$ with, for example, $v_{\text{min}} = -70\,\text{mV}$ and $v_{\text{max}} = 30\,\text{mV}$.

where τ_{close} and τ_{open} are the time constants with which the gate closes and opens and v_{gate} is the change-over voltage; throughout this paper we take $v_{\text{gate}} = 0.13$. With appropriate definitions of step functions $h_\infty(v)$ and $\tau(v)$, equation (4) may be written

$$\frac{dh}{dt} = \frac{h_\infty(v) - h}{\tau(v)}. \tag{5}$$

In more physiologically based models [e.g., Luo and Rudy (1991)], all gating variables satisfy equations of the form (5), but $h_\infty(v)$ and $\tau(v)$ are typically continuous functions of v.

The two-current model is similar in spirit to the FitzHugh–Nagumo model (FitzHugh, 1960, 1961), but we believe that the two-current model is more closely related to the physiology of the heart for two reasons. A minor issue: the two-current model does not exhibit voltage overshoot, a phenomenon observed in neural but not cardiac tissue. More importantly, the two-current model contains four time constants, which correspond to the four phases of the cardiac action potential: initiation, plateau, decay, and recovery. By contrast, the FitzHugh–Nagumo model has only two time constants. One of these constants is eliminated in the asymptotic approximation and the other merely defines the time scale of the action potentials; effectively, there are no dimensionless parameters in the FitzHugh–Nagumo model. However, in the two-current model, even after this reduction in the number of parameters, two dimensionless parameters remain. Different values of these parameters give rise to the various behaviors classified in Section 5 below.

3. ASYMPTOTIC DERIVATION OF THE RESTITUTION CURVE

In this section we derive an explicit leading-order asymptotic approximation for the restitution curve (this is defined in Section 3.2 below), based on the assumption[§] that

$$\tau_{\text{in}} \ll \tau_{\text{out}} \ll \tau_{\text{open}}, \tau_{\text{close}}. \tag{6}$$

According to (6), the time constants for the voltage equation (1) are much smaller than those in the gating variable equation (4). Therefore, changes in the voltage occur much faster than changes in the gating variable except possibly for points

---

[§]The assumption that $\tau_{\text{out}} \ll \tau_{\text{open}}, \tau_{\text{close}}$ does not hold for all physiological models: i.e., in many ionic models the time constants of a current may be comparable to the time constants of gates. If $\tau_{\text{out}}, \tau_{\text{open}}$, and τ_{close} are all comparable but much greater than τ_{in}, one may still apply asymptotic analysis to derive a map from the ODE's, but the derivation is harder and the results are not as clean. In keeping with the pedagogical goal of illustrating the use of asymptotic methods, we have restricted our attention to the simplest case that produces an excitable medium.

(a)

(b)
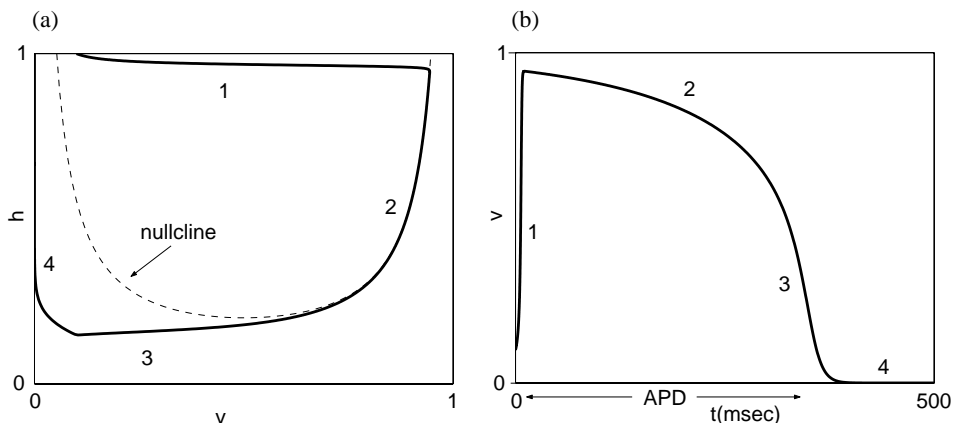
Figure 1. (a): Nullcline and trajectory of (1) and (4) in the h, v plane. The four stages of the action potential are labeled. (b): The voltage trace of the same action potential also showing the four stages. $\tau_{\text{close}} = 150$ ms, $\tau_{\text{open}} = 120$ ms, $\tau_{\text{out}} = 6$ ms, $\tau_{\text{in}} = 0.3$ ms, and $v_{\text{stim}} = 0.1$.

(v, h) near the nullclines of the voltage equation (1): i.e., assuming $J_{\text{stim}} = 0$, near solutions of

$$0 = \frac{hC(v)}{\tau_{\text{in}}} - \frac{v}{\tau_{\text{out}}}. \tag{7}$$

Apart from the trivial case $v = 0$, equation (7) expresses the condition that the inward and outward currents are exactly balanced. Solving this equation for h as a function of v yields

$$h = \frac{\tau_{\text{in}}}{\tau_{\text{out}}} \frac{v}{C(v)} = \frac{\tau_{\text{in}}}{\tau_{\text{out}}} \frac{1}{v(1-v)}; \tag{8}$$

and for v as a function of h,

$$v = v_{\pm}(h) = \frac{1}{2} \pm \sqrt{\frac{1}{4} - \frac{\tau_{\text{in}}}{\tau_{\text{out}}} h^{-1}}. \tag{9}$$

This nullcline is the dashed curve graphed in Fig. 1(a). Note that dv/dt is positive if $v_{-}(h) < v < v_{+}(h)$ and that dv/dt is negative in the complementary range $v < v_{-}(h)$ or $v > v_{+}(h)$. Defining h_{min} as the minimum value for h on this curve, we see from either (8) or (9) that

$$h_{\text{min}} = 4\frac{\tau_{\text{in}}}{\tau_{\text{out}}}. \tag{10}$$

3.1. *Response to a single stimulus.* Suppose that, starting from the stable equilibrium of equations (1) and (4) at $(v, h) = (0, 1)$, a brief stimulus current

is applied to increase the voltage. If the duration of the stimulus is short compared to τ_{in}, then the voltage rises to the value

$$v_{stim} \approx \int J_{stim}(t)dt, \tag{11}$$

and the change in h may be neglected. We assume that

$$v_{stim} > v_-(1) \tag{12}$$

where $v_-(h)$ is defined by (9): in words, that the state $(v_{stim}, 1)$ immediately following the stimulus current lies between the two branches of the nullcline (9) so that $dv/dt > 0$. Such a stimulus leads to an extended rise in the voltage known as an *action potential*. The following description of an action potential, based on assumption (6), identifies four phases, labeled 1–4 in Fig. 1.

  (i) Following the stimulus, J_{in} dominates J_{out}, and the voltage rises quickly to the nullcline $v = v_+(1)$. This occurs on a time scale of order τ_{in}, and the change in h during this time is negligible.
 (ii) As the gate closes according to equation (4), the voltage follows the nullcline, keeping the inward and outward currents balanced; thus, $v(t) = v_+(h(t))$. This occurs on a time scale of order τ_{close}.
(iii) When the gating variable reaches h_{min}, the solution 'falls off the nullcline': specifically, J_{out} dominates J_{in} and the voltage drops toward $v = 0$. This occurs on a time scale of order τ_{out}.
 (iv) The voltage stays small and the gate slowly reopens. The recovery has time constant τ_{open}, and it continues until the next stimulus is applied.

Frequently the fine structure of the action potential is ignored and it is described by only its duration. In this paper, we define[¶] the action potential duration (APD) to be the time during which the voltage is greater than v_{gate}. The voltage exceeds v_{gate} during phase 2 and during parts of phases 1 and 3. However, phases 1 and 3 are very brief—i.e., negligible in leading-order asymptotics—so the APD is approximately equal to the length of phase 2; i.e., the time required for h to decay from its initial value of $h = 1$ to $h = h_{min}$. Since h evolves according to equation (4), to leading order the APD is

$$\mathrm{APD_{max}} = \tau_{close} \ln\left(\frac{1}{h_{min}}\right). \tag{13}$$

As the notation $\mathrm{APD_{max}}$ suggests, (13) specifies the longest possible action potential duration.

3.2. *Multiple stimuli and the S1–S2 restitution curve.* Next we will explore the behavior of the model when, as illustrated in Fig. 2, it is stimulated twice in

---

[¶]In experiments the APD is often defined as the time during which the voltage is more than 10% of its maximum amplitude.
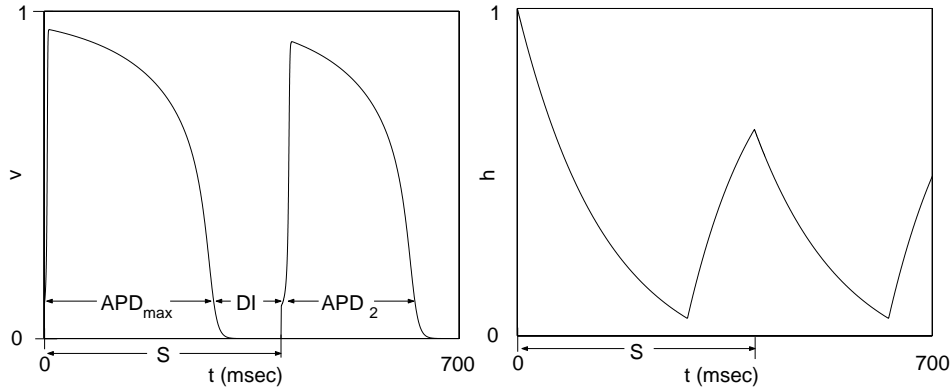
Figure 2. Voltage trace and gating variable, from (1) and (4), as functions of time, in response to two stimuli in sequence. Equation parameters are the same as in Fig. 1, and $S = 400$ ms.

sequence. Since we begin with fully recovered tissue (i.e., $v = 0$, $h = 1$), the first stimulus produces an action potential identical to the one described above; thus, its duration $\text{APD}_1 = \text{APD}_{\text{max}}$ is given by (13). If the first stimulus arrives at time $t = 0$ and the second at time $t = S$, then the time interval between the end of the first action potential and the arrival of the second stimulus, called the *diastolic interval*, is

$$\text{DI} = S - \text{APD}_1. \tag{14}$$

Below, using (6), we derive a function $F(\text{DI})$, with the property that the second action potential, in leading-order asymptotics, has duration

$$\text{APD}_2 \approx F(\text{DI}); \tag{15}$$

specifically, see (17). This function, or more properly its graph, is called the *restitution curve*.

The response to the second stimulus differs from the first because the system is not starting from equilibrium. Specifically, during phase 4 of the first action potential, i.e., for

$$\text{APD}_1 < t < S,$$

$v \approx 0$ and h satisfies (4) with initial condition $h = h_{\text{min}}$ at $t = \text{APD}_1$. Thus, at the arrival of the second stimulus,

$$h(S) = 1 - (1 - h_{\text{min}})e^{-\frac{\text{DI}}{\tau_{\text{open}}}}. \tag{16}$$

The second stimulus raises v to v_{stim} without changing h appreciably from (16).

If v_{stim} is large enough to generate a second action potential—see (19) below—we may also decompose the second action potential into four phases. During
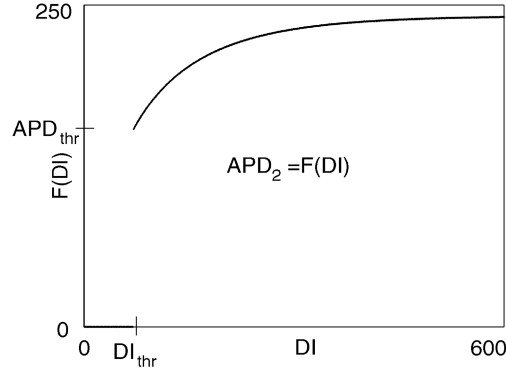
Figure 3. The restitution curve (17) derived from the 2-current model, including threshold behavior. Parameters are the same as in Fig. 1, so that $h_{\min} = 0.2$.

phase 1, the voltage rises rapidly to meet the nullcline at the point $(v_+(h(S)), h(S))$ while h remains essentially constant. During phase 2, (v, h) decays along the nullcline (9) from $h(S)$ to $h_{\min}$. Phases 3 and 4 are unchanged.

Now in leading-order asymptotics, APD_2 is the length of phase 2, i.e., the time required for h to decay from $h(S)$ to $h_{\min}$. Recalling (16), we obtain that $\text{APD}_2 \approx F(\text{DI})$ where

$$F(\text{DI}) = \tau_{\text{close}} \ln \left(\frac{1 - (1 - h_{\min})e^{-\frac{\text{DI}}{\tau_{\text{open}}}}}{h_{\min}} \right), \qquad (17)$$

which is graphed in Fig. 3. Incidentally, this restitution curve appears in Karma (1994). In the pedagogical spirit of this paper, we have derived (17) in detail.

For the second action potential to occur, the stimulus must raise the voltage sufficiently to pass the nullcline given in equation (8). For a particular stimulus strength there is a threshold value for the gate variable, say h_{thr}, such that if $h(S) > h_{\text{thr}}$ then an action potential will be elicited and if $h(S) < h_{\text{thr}}$ then the voltage will simply decay back towards zero. Indeed, h_{thr} is exactly the value of h on the nullcline (8) for $v = v_{\text{stim}}$: i.e.,

$$h_{\text{thr}} = \frac{\tau_{\text{in}}}{\tau_{\text{out}}} \frac{1}{v_{\text{stim}}(1 - v_{\text{stim}})} = \frac{h_{\min}}{4v_{\text{stim}}(1 - v_{\text{stim}})}. \qquad (18)$$

The time required, starting from $h_{\min}$, for the solution of (4) to reach h_{thr} gives a minimum value for DI

$$\text{DI}_{\text{thr}} = \tau_{\text{open}} \ln \left(\frac{1 - h_{\min}}{1 - h_{\text{thr}}} \right); \qquad (19)$$

the associated minimum APD is

$$\text{APD}_{\text{thr}} = \tau_{\text{close}} \ln \left(\frac{h_{\text{thr}}}{h_{\min}} \right). \qquad (20)$$
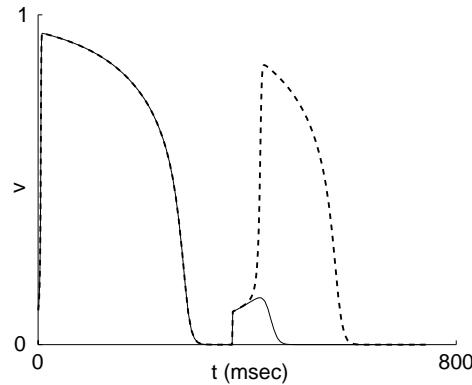
Figure 4. A pair of S1–S2 experiments that demonstrate the phenomenon of a threshold diastolic interval. The difference in DI in these two simulations is 0.01 m. For a DI of 84.25 ms, $APD_2 = 206.79$ ms (dashed curve), whereas for a DI of 84.24 m, only a subthreshhold response is produced (solid curve). (Before the second stimulus the two curves coincide.) Parameters are the same as in Fig. 1.

Therefore, in our asymptotic approximation, the restitution curve is given by equation (17) for $DI > DI_{thr}$ and is zero for $DI < DI_{thr}$, a discontinuous function, as illustrated in Fig. 3.

To justify our approximation of letting the restitution curve be discontinuous, we show in Fig. 4 a pair of simulations of the ODE (1) and (4) with diastolic intervals near DI_{thr}. An action potential is elicited with a DI of 84.25 ms but with a DI of only 0.01 ms shorter, the voltage never rises significantly above v_{stim}. We ignore the latter response, called a subthreshhold response, because such a voltage pulse would not propagate away from the stimulus site in a spatially extended model.

Remark. Our assumptions are intended to mimic the S1–S2 experimental protocol (Boyett and Fedida, 1984) in which the heart is paced slowly for several paces, allowing for full recovery, and then the APD following a premature stimulus is recorded. Although we consider only one preparatory action potential, our model is so simple that identical results would be obtained from multiple preparatory action potentials. Experimental data from this protocol is often fitted with a restitution function of the form [e.g., Nolasco and Dahlen (1968), Guevara *et al.* (1984), Glass and Mackey (1988)]

$$F(DI) = a - be^{-DI/c}. \tag{21}$$

In the limit of large DI, our function equation (17) assumes this form with $a = APD_{max}$, $b = \tau_{close}(1 - h_{min})$, and $c = \tau_{open}$. This may be seen using the approximation $\ln(1+z) \approx z$ for small z. However, (17) and (21) differ significantly at smaller DI. In Section 4, we shall use the mapping approximation (17) to study the effect of periodic stimulation on the models (1) and (4).
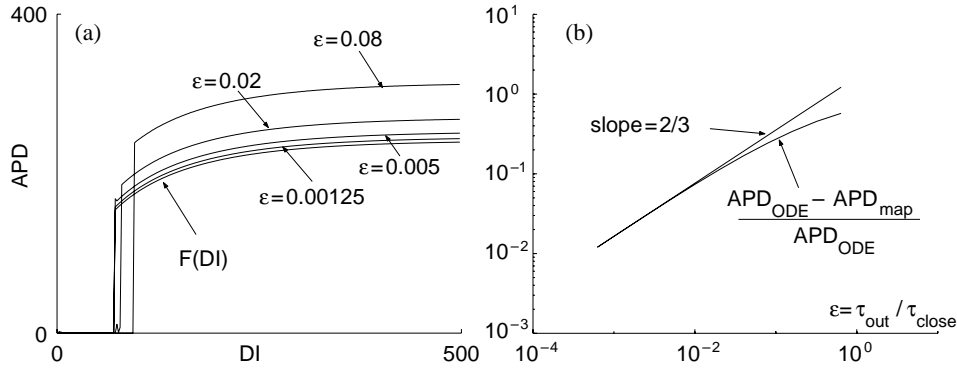
Figure 5. (a): S1–S2 restitution of (1) and (4) for several values of ϵ. The parameters τ_{close} and τ_{open} have the same values as in Fig. 1; and as ϵ varies, the ratio $\tau_{\text{in}}/\tau_{\text{out}}$ is held fixed at 0.05 (as in Fig. 1). The curves converge to the function (17) as $\epsilon \to 0$. (b): Relative error as a function of ϵ. This log–log plot has a slope of approximately 2/3 which confirms that the error in (17) is of order $\epsilon^{2/3}$.

3.3. *Accuracy of the asymptotic approximation.* In deriving (17), we neglected the time spent in phases 1 and 3 of the action potential. To discuss the accuracy of this approximation, we introduce the parameter

$$\epsilon = \frac{\tau_{\text{out}}}{\tau_{\text{close}}}, \tag{22}$$

a measure of how much shorter phase 3 is compared to phase 2. (Remark: As we shall see below, time spent in phase 1 is asymptotically negligible compared to time spent in phase 3.) Equation (17) is the leading order term in an asymptotic expansion as $\epsilon \to 0$ of the restitution curve. Figure 5(a) shows the restitution curves produced by solving the ODE (1) and (4) numerically in an S1–S2 protocol for several values of ϵ. The computed restitution curves indeed approach the mapping (17) as $\epsilon \to 0$, including the location and height of the jump at DI = DI$_{\text{thr}}$. These graphs illustrate a common feature of asymptotics: the qualitative prediction of asymptotic analysis usually remains correct far beyond the point where quantitative agreement begins to deteriorate.

To understand the deviation in Fig. 5(a) between (17) and the computed restitution curves for $\epsilon > 0$, it is necessary to examine higher-order terms in the asymptotic expansion. At first glance, one might propose an expansion in integral powers of ϵ. However, the transition from phase 2 to 3—'falling off the slow manifold'—is a singular phenomenon, and this may introduce fractional powers in the expansion. Indeed, as illustrated by the log–log plot [Fig. 5(b)] the first correction term has order $\epsilon^{2/3}$.

We may derive this exponent by a scaling argument modeled on the treatment (Bender and Orszag, 1978) of relaxation oscillations in Rayleigh's equation.

Following a stimulus at time $t = S$, equation (4) has the solution

$$h(t) = h(S)e^{-\frac{t-S}{\tau_{\text{close}}}} \tag{23}$$

where $h(S)$ is given by (16). Let t_* be the time at which (23) gives $h(t_*) = h_{\min}$; then we may rewrite (23) as

$$h(t) = h_{\min}e^{-\frac{t-t_*}{\tau_{\text{close}}}}. \tag{24}$$

Substituting (24) into (1) we obtain a nonautonomous equation for v for t in a neighborhood of t_*,

$$\frac{dv}{dt} = \frac{v}{\tau_{\text{out}}}\left(\frac{\tau_{\text{out}}}{\tau_{\text{in}}}h_{\min}e^{-\frac{t-t_*}{\tau_{\text{close}}}}v(1-v) - 1\right). \tag{25}$$

We do not know $v(t_*)$ exactly but we know from (9) that, since $h(t_*) = h_{\min} = 4\frac{\tau_{\text{in}}}{\tau_{\text{out}}}$, to leading order

$$v(t_*) \approx \tfrac{1}{2}. \tag{26}$$

To study the initial value problem (24) and (26) more carefully, let us introduce scaled variables

$$\bar{v} = \frac{v - \frac{1}{2}}{\epsilon^p}, \qquad \bar{t} = \frac{t - t_*}{\epsilon^q \tau_{\text{close}}}. \tag{27}$$

Note that we have nondimensionalized time with τ_{close}. We shall determine the appropriate exponents p and q by the principle of dominant balance (Bender and Orszag, 1978) as follows. Substituting (27) into (24), we obtain

$$\frac{\epsilon^p}{\epsilon^q \tau_{\text{close}}}\frac{d\bar{v}}{d\bar{t}} = \frac{1}{\tau_{\text{out}}}\left(\frac{1}{2} + \epsilon^p\bar{v}\right)\left(4e^{-\epsilon^q\bar{t}}\left(\frac{1}{2} + \epsilon^p\bar{v}\right)\left(\frac{1}{2} - \epsilon^p\bar{v}\right) - 1\right). \tag{28}$$

Expanding the exponential in (28) and recalling that $\epsilon = \tau_{\text{out}}/\tau_{\text{close}}$, we obtain, modulo higher order terms (i.e., ϵ^{2q}, ϵ^{p+q}, or ϵ^{3p}),

$$\epsilon^{1+p-q}\frac{d\bar{v}}{d\bar{t}} = -\frac{1}{2}\epsilon^q\bar{t} - 2\epsilon^{2p}\bar{v}^2. \tag{29}$$

To have dominant balance the three terms in (29) must all be of the same order: i.e.,

$$1 + p - q = q = 2p$$

which has solution $p = 1/3$, $q = 2/3$. Therefore, recalling (27), we see that the time required to cross the neighborhood of $v = 1/2$—to fall off the slow manifold—is of the order $\epsilon^{2/3}\tau_{\text{close}}$.

In more detail, for $\bar{t} < 0$ the two terms of the right-hand side (r.h.s.) of

$$\frac{d\bar{v}}{d\bar{t}} = -\frac{1}{2}\bar{t} - 2\bar{v}^2 \tag{30}$$
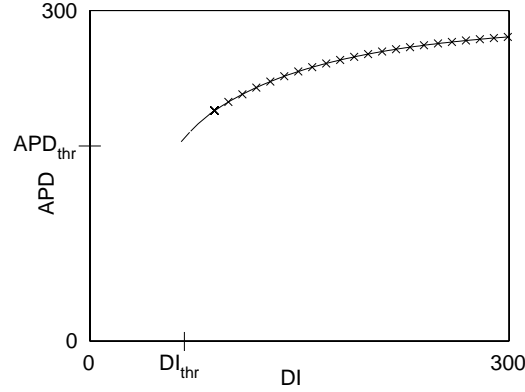
Figure 6. Comparison of dynamic and S1–S2 restitution curves for (1) and (4). The S1–S2 restitution is the solid line; the points on the dynamic curve are the *x*'s. Parameters are the same as in Fig. 1.

approximately balance as discussed above for phase 2. For $\bar{t} > 0$ the solution of (30) blows up in finite time; i.e., the voltage evolves rapidly to the region characterized above as phase 3. Following the treatment (Kevorkian and Cole, 1981) of Rayleigh's equation, one could continue this analysis to estimate the coefficient C in the series

$$\text{APD}_{\text{ODE}} = \text{APD}_{\text{map}} + C\epsilon^{2/3} \tag{31}$$

[notation as in Fig. 5(b)] but we have not pursued this rather tedious calculation.

4. DYNAMIC RESTITUTION

4.1. *Phenomenology.* Suppose that one stimulates a heart cell periodically, waits until it settles into a stable periodic response, and then records the APD. If the stimulation period is BCL (acronym for *basic cycle length*), then the diastolic interval in the periodic solution is

$$\text{DI} = \text{BCL} - \text{APD.} \tag{32}$$

With such a procedure one obtains a single point (APD, DI) on the so-called dynamic restitution curve.

To obtain the full dynamic restitution curve, one must perform this procedure repeatedly for various values of BCL. Typically one starts with a relatively long BCL and decreases BCL in small increments. Figure 6 shows the dynamic restitution curve for equations (1) and (4) for one set of parameter values obtained by simulating with this protocol (*x*'s), along with the S1–S2 restitution curve (solid line): the two curves essentially coincide. For a model as simple as (17), there is no meaningful difference in behavior in S1–S2 and dynamic restitution. We make
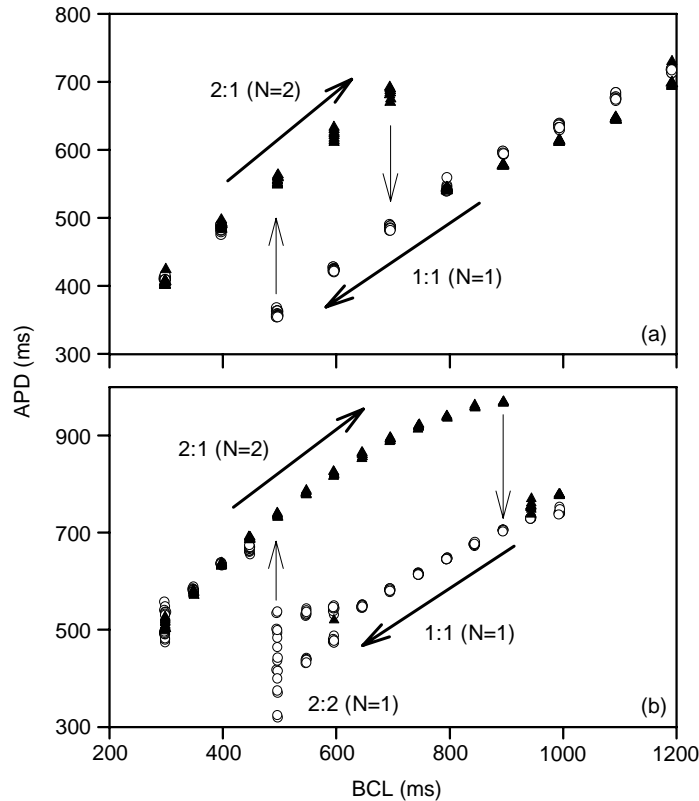
Figure 7. Dynamic restitution experiments with (lower plot) and without (upper plot) alternans (Hall *et al*., 1999).

the distinction purely as a pedagogical device. However, the distinction is very significant for experiments and more sophisticated models.

Note that the *x*'s in Fig. 6, points on the dynamic restitution curve, stop slightly above DI_{thr}. This is because at small DI the periodic solution is not stable. Exploration of this loss of stability is the main focus of this section. Incidentally, it is believed (Winfree, 1987; Karma, 1993) that this loss of stability is a precursor to the onset of arrhythmia.

At large BCL, and in particular for the simulation data shown in Fig. 6, each stimulus produces an action potential, which is called 1:1 behavior. As the BCL is decreased, this 1:1 behavior eventually becomes unstable. Possible behaviors beyond this loss of stability are suggested in Fig. 7, taken from the experiments of Hall *et al*. (1999) on small pieces of frog heart. For the animal illustrated in the upper figure, when BCL was decreased below the stability boundary, the heart evolved to what is called 2:1 behavior: i.e., only every other stimulus produced an action potential. In the figure the upper curve represents APD's measured for the 2:1 behavior. For the animal illustrated in the lower figure, 2:1 behavior also occurred for sufficiently small BCL, but what is called 2:2 behavior or *alternans*

occurred before $2:1$ behavior; this term means that every stimulus produced an action potential but the action potentials alternated between short and long in a periodic state of period $2 * \text{BCL}$. In the figure, alternans appear where the lower curve becomes double valued.

Following a sequence of experiments in which BCL was gradually decreased, Hall *et al.* (1999) then gradually increased BCL. In this way, they observed the hysteresis shown in the figures: i.e., for some values of BCL, both $1:1$ (or possibly alternans) and $2:1$ responses are possible, and which occurs depends on prior history.

4.2.   *Mathematical formulation.*   Graphs of APD vs. BCL, such as in Fig. 7, are called bifurcation diagrams. In this subsection we formulate equations that specify the bifurcation diagrams for our model, as described by the approximation (17). Bifurcation diagrams for the model, as compared to experiment, contain additional information in that unstable solutions may be included along with stable ones. In particular, we shall see that in situations where the model exhibits alternans (as in the lower plot of Fig. 7), a $1:1$ solution branch continues beyond the point where the $1:1$ response loses stability.

Let us consider the procedure for determining a point on the dynamic restitution curve in the context of the model (17). Suppose that, starting from equilibrium, stimuli are applied with period BCL, generating a sequence of action potentials of duration $\text{APD}_1, \text{APD}_2, \text{APD}_3, \ldots$. (For the moment we assume that every stimulus does generate an action potential.) From our discussion of the restitution curve in Section 3, we see that all the history before a given DI does not matter and that each new APD is determined by only the value of h at the time of stimulation, which in turn is determined by the length of DI: in symbols,

$$\text{APD}_{n+1} = F(\text{DI}_n), \tag{33}$$

where DI_n denotes the diastolic interval following APD_n. Since BCL is specified, we can replace DI_n in equation (33) with $\text{BCL} - \text{APD}_n$, so we have APD_{n+1} expressed as a function of APD_n. Calling this function Φ and recalling the definition (17) of F, we may write

$$\text{APD}_{n+1} = \Phi(\text{APD}_n) = \tau_{\text{close}} \ln \left(\frac{1 - (1 - h_{\min})e^{\frac{-\text{BCL}+\text{APD}_n}{\tau_{\text{open}}}}}{h_{\min}} \right). \tag{34}$$

In other words, the sequence of action potential durations is determined by iterations of the map Φ defined by (34).

As discussed as, for example, in Strogatz (1994), a fixed point of (34), by which we mean a solution of

$$\Phi(\text{APD}_*) = \text{APD}_*,$$
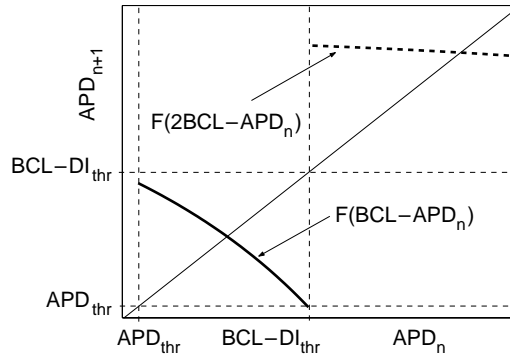
Figure 8. Graphical representation of fixed points of the mapping (34) (solid curve) and of (40) (dotted curve). Equation parameters are the same as in Fig. 1, and BCL = 450 ms.

represents a possible limit of the sequence $\{APD_n\}$. The solid curve in Fig. 8 shows a graph of Φ for BCL = 450 ms. [Although the notation $\Phi(APD_n)$ does not indicate it, the mapping to be iterated depends on BCL. When clarity requires, we shall write $\Phi(APD_n, BCL)$.] The intersection of this graph with the diagonal line $APD_{n+1} = APD_n$ is of course a fixed point of Φ. It is shown in Strogatz (1994) that a fixed point APD_* of the mapping Φ is stable if and only if[||]

$$|\Phi'(APD_*)| < 1. \tag{35}$$

A fixed point of Φ is associated with a $1:1$ response. An alternans response corresponds to a period-2 sequence of iterates, or equivalently a fixed point of the composed map $\Phi \circ \Phi$, which is defined by $\Phi \circ \Phi(APD) = \Phi(\Phi(APD))$. The equation for such fixed points may be written

$$\Psi(APD, BCL) = 0 \tag{36}$$

where Ψ is defined by

$$\Psi(A, B) = \Phi(\Phi(A, B), B) - A. \tag{37}$$

A brief calculation shows that a solution (APD, BCL) of (36) is stable if and only if

$$D_1\Psi(APD, BCL) < 0, \tag{38}$$

where $D_1\Psi$ denotes the partial derivative with respect to its first argument. Of course a fixed point of Φ is also a fixed point of $\Phi \circ \Phi$ and hence a solution of (36). Moreover, the stability (38) condition reduces to (35) in this case. Thus the single equation (36), a bifurcation problem of the type studied in Golubitsky and Schaeffer (1985), characterizes all $1:1$ and $2:2$ responses of our model. Moreover,

---

[||]More accurately, the fixed point is unstable if $|\Phi'(APD_*)| > 1$; and if $|\Phi'(APD_*)| = 1$, stability is determined by higher-order terms. Despite such subtleties, we shall describe conditions analogous to (35), as necessary and sufficient for stability.

this bifurcation problem has a reflectional or $\mathbb{Z}_2$ symmetry: if (APD, BCL) satisfies (36), then so does $(\Phi(\text{APD}), \text{BCL})$. We shall see in Section 5 that the transition from $1:1$ to $2:2$ behavior may be understood as a pitchfork bifurcation (Golubitsky and Schaeffer, 1985) of (36).

To describe $2:1$ responses, we need to relax our assumption that every stimulus produces an action potential. The issues here are related to the fact that in Fig. 8 we have graphed (34) (the dark curve) only on the interval $\text{APD}_{\text{thr}} < \text{APD}_n < \text{BCL} - \text{DI}_{\text{thr}}$. The lower limit simply represents the shortest possible action potential, but if the upper limit is violated, then the first stimulus after APD_n will arrive too soon to produce an action potential. In this case, assuming BCL is not excessively short, the next action potential will be produced by the second stimulus after APD_n, with diastolic interval [see Guevara *et al.* (1984)]

$$\text{DI} = 2\text{BCL} - \text{APD}_n. \tag{39}$$

Thus in Fig. 8, we have continued the graph in the range $\text{APD}_n > \text{BCL} - \text{DI}_{\text{thr}}$ by plotting (dashed line)

$$F(2\text{BCL} - \text{APD}_n). \tag{40}$$

Intersections of this dashed curve with the diagonal correspond to a $2:1$ response of the model. The equation for such intersections is

$$F(2\text{BCL} - \text{APD}) - \text{APD} = 0. \tag{41}$$

As in (35), a solution (APD, BCL) of equation (41) will be stable if and only if

$$|F'(2\text{BCL} - \text{APD})| < 1. \tag{42}$$

In conclusion, what we are calling a bifurcation diagram in this paper, the set of points (BCL, APD) that arise as $1:1$, $2:2$, or $2:1$ responses of the model, is a mathematical hybrid: i.e., a graph of the solutions of both (36) and (41) on one set of axes, along with indications of stability. Moreover, the discontinuity associated with the threshold of (34) at $\text{DI} = \text{DI}_{\text{thr}}$ gives rise to another nonstandard [compared to Golubitsky and Schaeffer (1985)] feature of the bifurcation diagrams considered here: because of it, a solution branch may terminate without any kind of bifurcation occurring, not even a limit point.

5. CLASSIFICATION OF BIFURCATION DIAGRAMS

5.1. *Formulation of results.* In this section we classify the qualitatively differ-ent[**] bifurcation diagrams that may arise from the system (1) and (4) for different

---

[**]The phrase *qualitatively different* is defined carefully in Golubitsky and Schaeffer (1985), but intuitive ideas about this concept, developed below, are quite sufficient for the present paper.

values of the parameters. [More accurately, we classify bifurcation diagrams that may arise from the asymptotic restitution curve (17). Through the application of the stability[††] results of Golubitsky and Schaeffer (1985), one can then extend the classification to (1) and (4), provided ϵ is sufficiently small.] We derive this information by purely analytical means, without recourse to simulations.

In presenting the classification, it is economical to combine the parameters in the model to form dimensionless parameters. The four time constants, τ_{in}, τ_{out}, τ_{open}, and τ_{close} can be combined to form three dimensionless ratios. Two such ratios have already been introduced: h_{min}, defined in equation (10), is proportional to $\tau_{\text{in}}/\tau_{\text{out}}$ and ϵ, defined in equation (22), equals $\tau_{\text{out}}/\tau_{\text{close}}$. As the third, let us define

$$r = \frac{\tau_{\text{open}}}{\tau_{\text{close}}}. \tag{43}$$

The model contains two additional parameters, v_{gate} in (4) and v_{stim} defined by (11). The dependence on v_{gate} is neither sensitive nor interesting, so we shall ignore this parameter. It is convenient to replace v_{stim} by h_{thr} which is the combination of v_{stim} and h_{min} defined in equation (18). By passage to the leading-order asymptotic limit (17), we have effectively removed ϵ. This leaves r, h_{thr}, and h_{min} as the essential dimensionless parameters, and in fact h_{min} plays only a secondary role. Note that r may lie anywhere in $(0, \infty)$ while h_{thr} and h_{min} are constrained to satisfy

$$0 < h_{\text{min}} < h_{\text{thr}} < 1. \tag{44}$$

For different parameter values, three qualitatively different bifurcation diagrams can arise in our model. The three cases, labeled α, β, and γ, are illustrated in Fig. 9; stable solution branches are shown as solid curves, unstable branches as dashed. The important features of these bifurcation diagrams are summarized in the two points below. To associate these bifurcation diagrams with specific parameter values, we refer to the three regions, labeled α, β, γ, of the r, h_{thr}-plane identified in Fig. 10. We shall show that *for all values of (r, h_{thr}) in one of these regions, the bifurcation diagram is qualitatively similar to the corresponding diagram illustrated in Fig. 9*. In the proof we shall also show that the lower edge of Region α has the equation

$$h_{\text{thr}} = \frac{1}{r+1}, \tag{45}$$

and the boundary between Regions β and γ has the equation

$$r = 1, \qquad 0 < h_{\text{thr}} < \tfrac{1}{2}. \tag{46}$$

To articulate the first point, let us define

$$\text{BCL}_{\text{thr}} = \text{APD}_{\text{thr}} + \text{DI}_{\text{thr}}, \tag{47}$$

[††]This is a different notion of stability from stability of an equilibrium as characterized, for example, by (35); it has to do with the structural stability of equation (36). See Golubitsky and Schaeffer (1985) for further discussion.
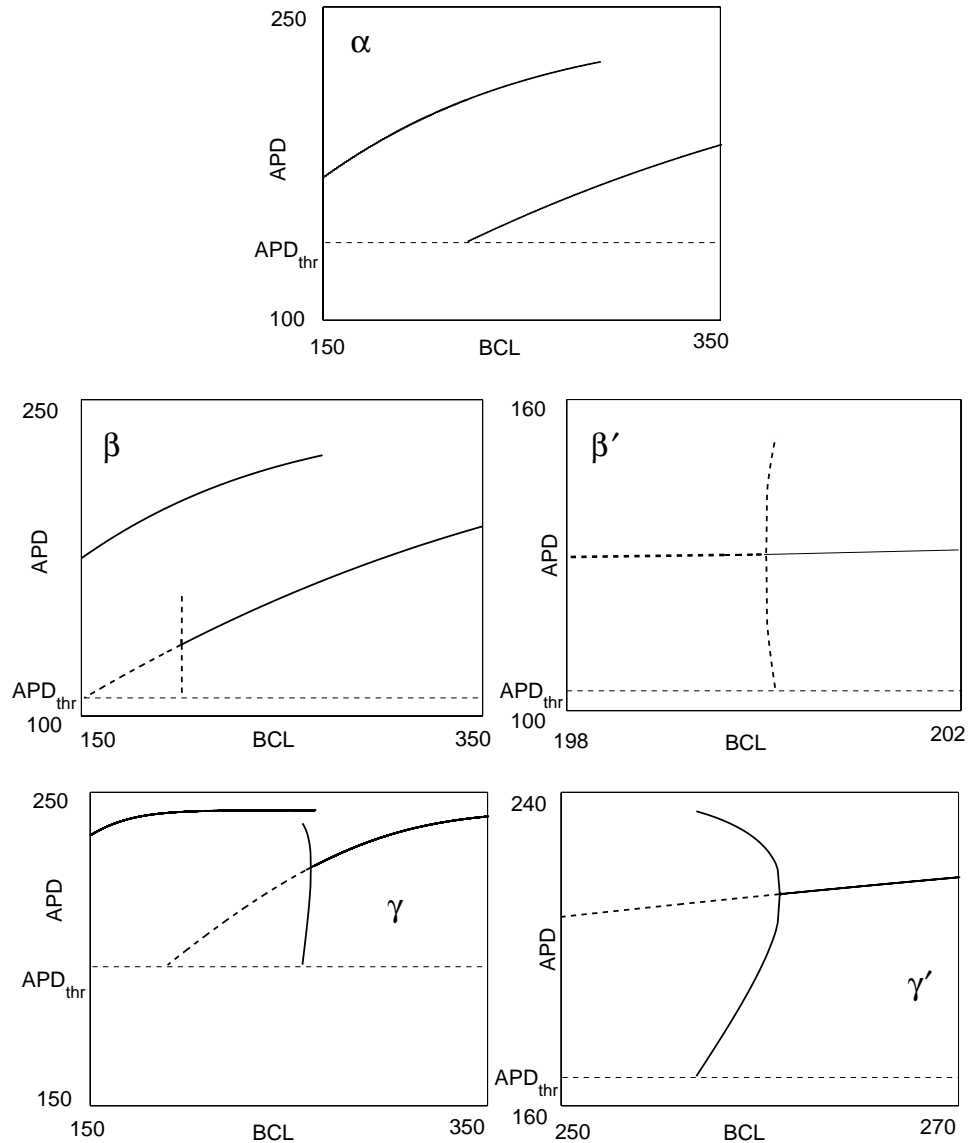
Figure 9. Three qualitatively different bifurcation diagrams. In all cases, $\tau_{\text{close}} = 150$ and $h_{\min} = 0.2$. α: The $1:1$ solution ceases to exist due to the threshold. $r = 1.2$ and $h_{\text{thr}} = 0.5$. β: The $1:1$ solution loses stability through a subcritical bifurcation. The unstable $1:1$ and alternans solutions are shown by dotted lines. $r = 1.1$ and $h_{\text{thr}} = 0.4$. β': Blow-up of the bifurcation region, showing that the bifurcation is subcritical. γ: The $1:1$ solution undergoes a supercritical bifurcation resulting in stable alternans solutions and an (dotted line) unstable $1:1$ solution. $r = 0.2$ and $h_{\text{thr}} = 0.6$. γ': Blow-up of the bifurcation region.

where APD_{thr} and DI_{thr} are given by (19) and (20), respectively. BCL_{thr} is the shortest BCL at which it is possible for every stimulus to produce an action potential.
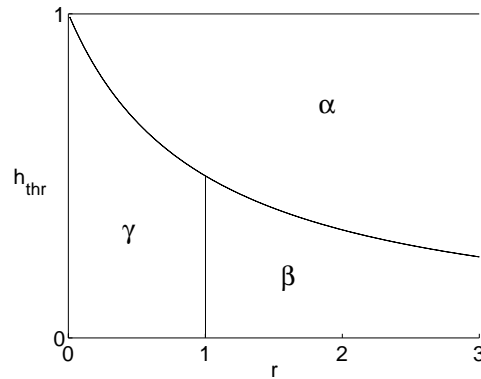
Figure 10. Regions in parameter space in which the different bifurcation diagrams of Fig. 9 occur.

Point 1. (a) In Case α, the $1:1$ response is stable for all $\text{BCL} > \text{BCL}_{\text{thr}}$, while for Cases β and γ the $1:1$ response loses stability through a pitchfork bifurcation of (36) at $\text{BCL} = \text{BCL}_{\text{bif}}$, where $\text{BCL}_{\text{bif}} > \text{BCL}_{\text{thr}}$, at which alternans (or $2:2$) solutions appear. [Equation (55) below gives a formula for BCL_{bif}.] (b) In Case β the bifurcating $2:2$ solutions are unstable, while in Case γ they are stable.

Adapting the usual terminology that is derived from fluid mechanics, we will call the bifurcation diagram illustrated in Case β *subcritical*; in Case γ, *supercritical*.

Implications for experiment. The simple exponential map (21) exhibits only the behavior of Cases α and γ. These two cases are familiar from the literature—as BCL is decreased, either the response jumps abruptly from $1:1$ to $2:1$ (in Case α) or such a jump occurs following an interval of alternans (Case γ). Case β is new: the transition from $1:1$ to $2:1$ occurs as a result of a bifurcation rather than of DI falling below a threshold. This different mechanism has two consequences:

- In Case β, the evolution to $2:1$ behavior involves a long transient during which the APD alternates between slightly shorter and slightly longer APD's than the $1:1$ response, while in Case α, the $2:1$ behavior establishes itself immediately.
- In Case β, the location of the $1:1$-to-$2:1$ transition would not be affected by stimulus strength. By contrast, at least in our model, DI_{thr} depends on stimulus strength, so that in Case α one may extend the range of the $1:1$ response by increasing the stimulus strength.

It would be interesting to examine more detailed ionic models and experimental data for either of these signs of the behavior of Case β.

To articulate the second point, let us define BCL_{max2} as the longest basic cycle length such that the $2:1$ solution exists. Similarly, we define BCL_{min1} as the shortest basic cycle length such that either a $1:1$ or $2:2$ response exists and is

stable[‡‡]. In Case α, $\text{BCL}_{\text{min1}} = \text{BCL}_{\text{thr}}$; in Case β, $\text{BCL}_{\text{min1}} = \text{BCL}_{\text{bif}}$; and in Case γ, BCL_{min1} is characterized by the property that the shorter of the diastolic intervals in the $2:2$ response equals DI_{thr}.

Point 2. The $2:1$ solution exists and is stable in an interval that contains BCL_{min1}. In symbols,

$$\text{BCL}_{\text{min1}} < \text{BCL}_{\text{max2}}, \tag{48}$$

and the $2:1$ response is stable for $\text{BCL}_{\text{min1}} < \text{BCL} < \text{BCL}_{\text{max2}}$.

Implications for experiment. As regards experiments, Point 2 implies that in all three cases there is hysteresis in the bifurcation diagram. The $2:1$ solution does lose stability at sufficiently small BCL, but, according to Point 2, this occurs for BCL below BCL_{min1}.

Incidentally, although we do not prove it here, a further distinction in behavior arises in Case γ. It may happen that the $2:1$ solution branch ends at a value of BCL greater than the bifurcation point, where the $1:1$ branch is still stable; in symbols

$$\text{BCL}_{\text{bif}} < \text{BCL}_{\text{max2}}. \tag{49}$$

However, the reverse inequality is also possible. Experimentally, this distinction would manifest itself during the upsweep of BCL when the $2:1$ response loses stability, specifically in whether the system falls back to a $1:1$ response or a $2:2$ response. To be precise, (49) holds for a parameter choice (r, h_{thr}) belonging to Region γ if and only if

$$\begin{aligned} &\text{(i)} \quad 1 - r(r+1)^{\frac{1}{r}-1} < h_{\text{thr}} \quad \text{and} \\ &\text{(ii)} \quad h_{\text{min}} \text{ is sufficiently small.} \end{aligned} \tag{50}$$

5.2. *Proofs of the above two claims.*

Proof of point 1a. The $1:1$ solution bifurcates when (35) is violated. Let us write DI_{bif} for the diastolic interval associated with the first violation of (35). Differentiating equation (34) and setting the absolute value of the derivative equal to one gives the relation

$$|\Phi'| = \frac{1}{r} \frac{(1 - h_{\text{min}})e^{-\text{DI}_{\text{bif}}/\tau_{\text{open}}}}{1 - (1 - h_{\text{min}})e^{-\text{DI}_{\text{bif}}/\tau_{\text{open}}}} = 1. \tag{51}$$

[‡‡]Such significant values for BCL can be estimated using the formulas that appear in the proofs below. Although we show that the *qualitative* form of the bifurcation is the same for all r, h_{thr} in a given region of Fig. 10, quantitatively the numerical values of these parameters vary considerably over the region. Using the formulas for these parameters, one could address questions such as 'What parameter values in a region maximize the interval in which stable $1:1$ and $2:1$ responses overlap?' Despite the interest of such questions, we do not pursue them here.

We write h_{bif} for the denominator in (51),

$$h_{\text{bif}} = 1 - (1 - h_{\text{min}})e^{-\text{DI}_{\text{bif}}/\tau_{\text{open}}}, \tag{52}$$

since this is the value to which h recovers during the time DI_{bif}. Reexpressing (51) in terms of h_{bif}, we obtain

$$\frac{1 - h_{\text{bif}}}{r h_{\text{bif}}} = 1, \tag{53}$$

which may be solved for h_{bif} to give

$$h_{\text{bif}} = \frac{1}{r + 1}. \tag{54}$$

For the solution to remain stable until it ceases to exist at $\text{DI} = \text{DI}_{\text{thr}}$ (as claimed for Region α), we must have $\text{DI}_{\text{bif}} < \text{DI}_{\text{thr}}$. This equation may be reexpressed in terms of h as $h_{\text{bif}} < h_{\text{thr}}$. Recalling (54), we see that such behavior occurs if $1/(r + 1) < h_{\text{thr}}$. Conversely, if the reverse inequality holds, then the solution loses stability before it ceases to exist (as claimed for Regions β and γ). The boundary between these two behaviors is the curve (45), which completes the proof of Point 1a.

Remark. At the bifurcation point,

$$\text{BCL}_{\text{bif}} = \tau_{\text{close}}\ln\frac{h_{\text{bif}}}{h_{\text{min}}} + \tau_{\text{open}}\ln\frac{1 - h_{\text{min}}}{1 - h_{\text{bif}}}, \tag{55}$$

where h_{bif} is given by (54).

Proof of point 1b. To start, we want to determine the parameter values at which the bifurcation changes from supercritical to subcritical. Without much calculation, one can see that such a transition takes place for $r = 1$, as follows. If $r = 1$, then by (54), $h_{\text{bif}} = 1/2$; and by (55),

$$\text{BCL}_{\text{bif}} = \tau_*\ln\left(\frac{1 - h_{\text{min}}}{h_{\text{min}}}\right)$$

where τ_* denotes the common value of τ_{close} and τ_{open}. Substituting into (34) we obtain, for $\text{BCL} = \text{BCL}_{\text{bif}}$,

$$\text{APD}_{n+1} = \tau_*\ln\left(\frac{1 - h_{\text{min}}e^{\text{APD}_n/\tau_*}}{h_{\text{min}}}\right),$$

and this may be rewritten in the symmetric form

$$h_{\text{min}}e^{\text{APD}_{n+1}/\tau_*} + h_{\text{min}}e^{\text{APD}_n/\tau_*} = 1.$$

Applying this form twice we see that $\text{APD}_{n+2} = \text{APD}_n$, or $\Phi \circ \Phi$ is the identity. In other words, when $r = 1$, all the bifurcating solutions are contained in the 'vertical' line

$$\{(\text{APD}, \text{BCL}) : \text{BCL} = \text{BCL}_{\text{bif}}\},$$

a bifurcation that is neither subcritical nor supercritical. Incidentally, since

$$(\Phi \circ \Phi)'(\text{APD}_n) = 1, \tag{56}$$

all these $2:2$ solutions are neutrally stable.

During alternans, every other action potential has the same duration; thus we define APD_{odd} and APD_{even} and rewrite (36) as the system

$$\begin{aligned}\Phi(\text{APD}_{\text{odd}}, \text{BCL}) - \text{APD}_{\text{even}} &= 0 \\ \Phi(\text{APD}_{\text{even}}, \text{BCL}) - \text{APD}_{\text{odd}} &= 0.\end{aligned} \tag{57}$$

To examine the transition from subcritical to supercritical more closely, we apply the Liapunov–Schmidt reduction (Golubitsky and Schaeffer, 1985) to the system (57). Specifically, we define the variable $x = \text{APD}_{\text{even}} - \text{APD}_{\text{odd}}$ and reduce the system (57) to a single equation

$$g(x, \text{BCL}) = 0 \tag{58}$$

with one unknown x and the parameter BCL. (In calculating derivatives below we shall abbreviate BCL to B.) Note that, since (57) is invariant under exchange of APD_{odd} and APD_{even}, the reduced function g is odd in x: i.e., $g(-x, B) = -g(x, B)$. In particular, $x = 0$ is a solution of (58) for all B; these 'trivial' solutions correspond to a $1:1$ response. The solutions corresponding to a $2:2$ response bifurcate from the trivial solution at a point where the derivative of (58) vanishes; in symbols $g_x = 0$. Whether the bifurcation is subcritical or supercritical is determined by the sign of the product $g_{xxx}g_{xB}$. Using equation (3.23) on page 33 of Golubitsky and Schaeffer (1985) we can compute that, at the bifurcation point,

$$g_{xxx} = 2F'''(\text{DI}_{\text{bif}}) - 3(F''(\text{DI}_{\text{bif}}))^2 \tag{59}$$

and

$$g_{xB} = F''(\text{DI}_{\text{bif}}). \tag{60}$$

Since F is concave downward, $g_{xB} < 0$. A straightforward calculation gives

$$F''(\text{DI}_{\text{bif}}) = -\frac{r+1}{\tau_{\text{open}}} \tag{61}$$

and

$$F'''(\text{DI}_{\text{bif}}) = \frac{(2r+1)(r+1)}{\tau_{\text{open}}^2} \tag{62}$$

where we have substituted for h_{bif} using equation (54). Plugging equations (61) and (62) into (59) and simplifying we have

$$g_{xxx} = \frac{r^2 - 1}{\tau_{\text{open}}^2}. \tag{63}$$
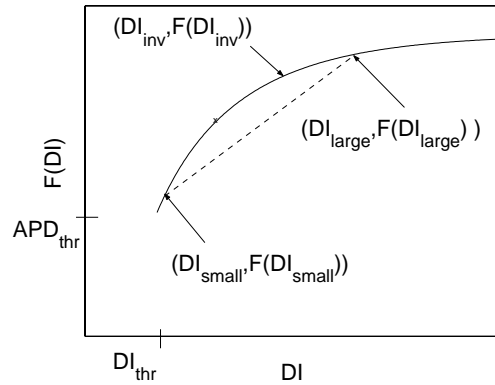
Figure 11. A construction in the proof of Point 1b. In this figure $DI_{inv} < DI_{large}$, which corresponds to Case γ.

If $r > 1$, then $g_{xxx}g_{xB} < 0$, so the bifurcating solutions exist for $BCL > BCL_{bif}$, as illustrated in Fig. 9β. Similarly, a bifurcation diagram of the form illustrated in Fig. 9γ arises if $r < 1$.

By exchange of stability [see Golubitsky and Schaeffer (1985)], we deduce that *near the bifurcation point*, the 2:2 solutions are unstable in Case β, stable in Case γ. We will complete the proof by showing that *any* 2:2 solution in Case β is unstable, and *any* 2:2 solution in Case γ is stable. Consider a 2:2 solution in which long and short action potentials alternate. Let DI_{small} and DI_{large} be the shorter and longer diastolic intervals, respectively. This 2:2 solution will be stable if and only if $F'(DI_{small})F'(DI_{large}) < 1$, or equivalently,

$$F'(DI_{large}) < 1/F'(DI_{small}). \tag{64}$$

If we define DI_{inv} ('inv' for inverse) in terms of the r.h.s. of (64),

$$F'(DI_{inv}) = 1/F'(DI_{small}), \tag{65}$$

then (64) is equivalent to

$$F'(DI_{large}) < F'(DI_{inv}), \tag{66}$$

which in turn is equivalent to an inequality on the slopes of the two chords passing through $(DI_{small}, F(DI_{small}))$ (see Fig. 11)

$$\frac{F(DI_{large}) - F(DI_{small})}{DI_{large} - DI_{small}} < \frac{F(DI_{inv}) - F(DI_{small})}{DI_{inv} - DI_{small}}. \tag{67}$$

Now

$$DI_{large} + F(DI_{small}) = +DI_{small} + F(DI_{large})$$

(since both sides equal BCL), and it follows that the slope on the left-hand side of equation (67) equals 1. Let

$$h_{\text{small}} = 1 - (1 - h_{\text{min}})e^{-\frac{\text{DI}_{\text{small}}}{\tau_{\text{open}}}}, \qquad h_{\text{inv}} = 1 - (1 - h_{\text{min}})e^{-\frac{\text{DI}_{\text{inv}}}{\tau_{\text{open}}}};$$

then equation (67), with the left-hand side replaced by unity, can be rewritten

$$\tau_{\text{close}}\ln\left(\frac{h_{\text{inv}}}{h_{\text{small}}}\right) > \tau_{\text{open}}\ln\left(\frac{1 - h_{\text{small}}}{1 - h_{\text{inv}}}\right). \tag{68}$$

Recalling the definition of DI_{inv},

$$F'(\text{DI}_{\text{small}})F'(\text{DI}_{\text{inv}}) = \frac{1 - h_{\text{small}}}{rh_{\text{small}}}\frac{1 - h_{\text{inv}}}{rh_{\text{inv}}} = 1, \tag{69}$$

we can solve for h_{inv} as a function of h_{small}

$$h_{\text{inv}} = \frac{1 - h_{\text{small}}}{1 - h_{\text{small}}(1 - r^2)}. \tag{70}$$

Substituting equation (70) into (68), exponentiating and simplifying gives the condition for stability

$$r^{2r}\frac{\left(\frac{h_{\text{small}}}{1 - h_{\text{small}}}\right)^{r-1}}{(1 - h_{\text{small}}(1 - r^2))^{r+1}} > 1. \tag{71}$$

We claim that (71) is satisfied if (h_{thr}, r) belongs to Region γ, and is violated if (h_{thr}, r) belongs to Region β. First note from Fig. 11 that $\text{DI}_{\text{thr}} < \text{DI}_{\text{small}} < \text{DI}_{\text{bif}}$, and it follows that $h_{\text{thr}} < h_{\text{small}} < h_{\text{bif}}$. Thus, recalling (45) and (54), we see that (h_{small}, r) belongs to Region β if and only if (h_{thr}, r) belongs to Region β, and likewise for Region γ. Let us write l.h.s. for the left-hand side of (71). Observe that l.h.s. equals unity if either $r = 1$ or if $h_{\text{small}} = \frac{1}{r+1} = h_{\text{bif}}$; i.e., l.h.s. = 1 for (h_{small}, r) on the boundaries of Regions β and γ. To estimate l.h.s. for (h_{small}, r) in the interior of these regions, we move away from the boundary $h_{\text{small}} = \frac{1}{r+1}$ by *decreasing* h_{small} while holding r fixed. One can show by a straightforward calculation that the derivative of l.h.s. with respect to h_{small} is a positive quantity times $(r - 1)$. Therefore, in Region γ, where $r < 1$, l.h.s. >1 and the solution is stable; similarly the solution is unstable in Region β.

Proof of point 2. In the proof we shall use the inequality that for a $1:1$ solution

$$\text{BCL} - \text{APD} > \text{DI}_{\text{thr}}; \tag{72}$$

this holds because, if (72) were violated, the following diastolic interval would be so short that the next stimulus could not generate an action potential. For a $2:2$ solution, both the shorter and longer action potentials must satisfy (72). For a $2:1$ solution, similar reasoning leads to the conclusion that

$$\text{BCL} - \text{APD} < \text{DI}_{\text{thr}}. \tag{73}$$

We begin by characterizing the maximum $2:1$ solution as follows: In the limiting case of $\text{BCL} = \text{BCL}_{\text{max2}}$, inequality (73) degenerates into the equality
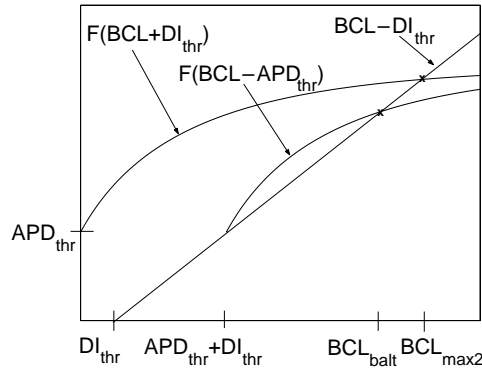
Figure 12. Graphical solution of equations (74) and (75). The independent variable is BCL.

$$BCL - APD = DI_{thr}.$$

Since $APD = F(DI)$, where $DI = 2BCL - APD = BCL + DI_{thr}$, we may rearrange terms in the displayed equation to conclude

$$BCL_{max2} - DI_{thr} = F(BCL_{max2} + DI_{thr}). \tag{74}$$

The upper curve in Fig. 12 illustrates a graphical solution of this equation.

An analogous characterization of BCL_{min1} depends on which region of the r, h_{thr}-plane the parameters lie in, so we consider the three cases separately. In Case α,

$$BCL_{min1} - DI_{thr} = BCL_{thr} - DI_{thr} = APD_{thr},$$

and the observation that $F(BCL_{max2} + DI_{thr}) > APD_{thr}$ implies that (48) is satisfied.

In Cases β and γ, let BCL_{balt} be the BCL at which the difference between even and odd action potential durations is maximal: i.e., the *boundary* of the interval of BCL's in which the alternans response exists. Then, passing to the limit of a rearranged version of (72), we conclude that

$$BCL_{balt} - DI_{thr} = F(BCL_{balt} - APD_{thr}). \tag{75}$$

The lower curve in Fig. 12 illustrates a graphical solution of (75), and it may be seen from the figure that $BCL_{balt} < BCL_{max2}$. In Case γ, $BCL_{balt} = BCL_{min1}$ so (48) holds; in Case β, we have

$$BCL_{min1} < BCL_{balt} < BCL_{max2},$$

which verifies (48) in all cases.

Now we show that for any BCL such that the $2:1$ solution exists and either a $2:2$ or $1:1$ solution is stable, the $2:1$ solution is also stable. If we are dealing with a

stable $1:1$ solution, let DI_1 and DI_2 be the diastolic intervals of the $1:1$ and $2:1$ solutions, respectively. Equations (72) and (73) can be rewritten

$$F(DI_1) < BCL - DI_{thr}$$

and

$$F(DI_2) > BCL - DI_{thr}$$

respectively and we conclude that, since F is monotone increasing,

$$DI_1 < DI_2.$$

Since $F'(DI)$ is monotone decreasing, it follows that

$$F'(DI_2) < F'(DI_1) < 1,$$

the latter inequality because the $1:1$ solution was assumed to be stable. Hence, the $2:1$ solution is also stable. If we are dealing with a stable $2:2$ solution, we replace DI_1 by DI_{large}, the longer of the two diastolic intervals, and we repeat the preceding argument with a minor elaboration at the last step: we argue that $F'(DI_{large}) < 1$ because by stability $F'(DI_{large})F'(DI_{small}) < 1$ and by monotonicity $F'(DI_{large}) < F'(DI_{small})$.

ACKNOWLEDGEMENTS

REFERENCES

Banville, I. and R. Gray (2002). Effect of action potential duration and conduction velocity restitution and their spatial dispersion on alternans and the stability of arrhythmias. *J. Cardiovasc. Electrophysiol.* **13**, 1141–1149.

Beeler, G. and H. Reuter (1977). Reconstruction of the action potential of ventricular myocardial fibres. *J. Physiol. (Lond.)* **268**, 177–210.

Bender, C. and S. Orszag (1978). *Advanced Mathematical Methods for Scientists and Engineers*, McGraw-Hill.

Boyett, M. and D. Fedida (1984). Changes in the electrical activity of dog cardiac Purkinje fibres at high heart rates. *J. Physiol.* **350**, 361–391.

Euler, D. (1999). Cardiac Alternans: Mechanisms and pathophysiological significance. *Cardiovasc. Res.* **42**, 583–590.

Fenton, F. and A. Karma (1998). Vortex dynamics in three-dimensional continuous myocardium with fiber rotation: Filament instability and fibrillation. *Chaos* **8**, 20–47.

FitzHugh, R. (1960). Thresholds and plateaus in the Hodgkin–Huxley nerve equations. *J. Gen. Physiol.* **43**, 867–896.

FitzHugh, R. (1961). Impulse and physiological states in models of nerve membrane. *Biophys. J.* **1**, 445–466.

Gilmour, R., N. Otani and M. Watanabe (1997). Memory and complex dynamics in cardiac Purkinje fibers. *Am. J. Physiol.* **272**, 1826–1832.

Glass, L. and M. Mackey (1988). *From Clocks to Chaos: The Rhythms of Life*, Princeton University Press.

Golubitsky, M. and D. Schaeffer (1985). *Singularities and Groups in Bifurcation Theory*, Vol. I, Springer.

Guevara, M., M. Ward, A. Shrier and L. Glass (1984). Electrical alternans and period-doubling bifurcations. *Comput. Cardiology* 167–170.

Hall, G. M., S. Bahar and D. Gauthier (1999). Prevalence of rate-dependent behaviors in cardiac muscle. *Phys. Rev. Lett.* **82**, 2995–2998.

Karma, A. (1993). Spiral breakup in model equations of action potential propagation in cardiac tissue. *Phys. Rev. Lett.* **71**, 1103–1106.

Karma, A. (1994). Electrical alternans and sprial wave breakup in cardiac tissue. *Chaos* **4**, 461–472.

Kevorkian, J. and J. Cole (1981). *Perturbation Methods in Applied Mathematics*, Springer.

Luo, C. and Y. Rudy (1991). A model of the ventricular cardiac action potential. *Circ. Res.* **68**, 1501–1526.

Luo, C. and Y. Rudy (1994). A dynamic model of the cardiac ventricular action potential. *Circ. Res.* **74**, 1071–1096.

Noble, D. (1960). Cardiac action and pacemaker potentials based on the Hodgkin–Huxley equations. *Nature* **188**, 495–497.

Noble, D. (1962). A modification of the Hodgkin–Huxley equations applicable to purkinje fibre action potentials. *J. Physiol.* **160**, 317–352.

Nolasco, J. and R. Dahlen (1968). A graphic method for the study of alternation in cardiac action potentials. *J. Appl. Physiol.* **25**, 191–196.

Strogatz, S. (1994). *Nonlinear Dynamics and Chaos*, Addison Wesley.

Tolkacheva, E., D. Schaeffer, D. Gauthier and C. Mitchell (2002). Analysis of the Fenton–Karma model through approximation by a one dimensional map. *Chaos* **12**, 1034–1042.

Winfree, A. (1987). *When Time Breaks Down: The Three-Dimensional Dynamics of Electrochemical Waves and Cardiac Arrhythmias*, Princeton University Press.